npj | clean water

Article

Published in partnership with King Fahd University of Petroleum & Minerals

https://doi.org/10.1038/s41545-024-00330-9

Synchronization of Ti_3C_2 MXene/Fe^{3+} with sodium persulfate for the degradation of reactive dyes

Wanxin Li[1], Dawu Shu[1,2] ✉, Fangfang An[1] ✉, Ruigang Liu[2], Juchuan Shan[1], Bo Han[1] & Shaolei Cao[1]

Rapid activation of sodium persulfate (SPS) for the degradation of C.I. Reactive Red 218 (RR218) was achieved using Ti_3C_2 MXene reduction of trace Fe^{3+}. The degradation rate of RR218 reached 97.7% using a mixture containing 3 g L^{-1} of SPS, 3.35 mg L^{-1} of Fe^{3+} and 60 mg L^{-1} of MXene stirred at 25 °C for 30 min. The intense reduction of Ti_3C_2 MXene triggers the Fe^{3+}/Fe^{2+} cycle thereby accelerating the activation of SPS. When reactive dyes were degraded by Fe^{3+}/SPS/MXene process, ·OH played a major role. The dye degradation capacity of the Fe^{3+}/SPS/MXene process decreased after 5 cycles of recycling. In addition, the wastewater treated under these conditions resulted in high dyeing efficiencies in reuse experiments. This study not only improves the understanding of the catalytic reaction of MXene but also provides a wastewater treatment and reuse process with low metal consumption and high efficiency.

Printing and dyeing industry is not only an important part of the textile economy but also a highly polluting manufacturing sector[1,2]. As far as reactive dyeing is concerned, wastewater contains a large number of dyes, additives, salts, and other chemical substances, which are characterized by high chromaticity, high content of inorganic salts, heavy metals, and organic compounds[3]. Therefore, the direct discharge of dyeing wastewater seriously threatens the ecological environment and human health[4–7].

At present, many researchers have conducted an extensive study on the treatment of dyeing wastewater, forming advanced oxidation technologies such as Ozone, Fenton, Permanganate, and Persulfate[8–11]. Among them, the advanced peroxidation technology based on persulfate to realize efficient treatment of printing and dyeing wastewater relies on the generation of reactive oxygen species such as sulfate radicals ($SO_4^{\bullet-}$) and hydroxyl radicals (·OH) by breaking the peroxyl bond[12]. Heat, alkali, ultrasound and transition metals are all effective ways to activate perovskites to achieve O-O fracture. Thermally activated persulphates are proficient at degrading down monomers or small molecules but encounter difficulties in treating aggregates or large molecules[13–15]. Under alkaline conditions, reactive dyes exist in the form of aggregates, which are difficult to collide effectively with free radicals. Therefore, dyeing wastewater is treated inefficiently under alkaline conditions[16]. Ultrasonic activation improves the efficiency of wastewater treatment by turbulence and higher $SO_4^{\bullet-}$. However, too much power reduces the cavitation of the solution, which is not conducive to the removal of organic matter[17]. Fe^{2+} among transition metals is widely used in persulfate advanced oxidation technology, but it cannot avoid problems such as sludge and increased chroma[18]. Chemical and electrochemical methods are mainly used for the reduction of Fe^{3+}. Chemicals such as hydroxylamine and ascorbic acid are used to reduce Fe^{3+}, though there are potential safety risks[19]. In addition, Fe^{3+} can be reduced to Fe^{2+} through electrodes. Nevertheless, the electrode is easily worn out, and the anode may produce harmful substances, which cannot be avoided[20].

MXene materials have a high specific surface area and a large number of functional groups, giving them strong reducing properties[21,22]. The surface of the exfoliated monolayer $Ti_3C_2T_x$ MXene material (T stands for surface terminated functional groups (e.g., -OH, -O, -F), and X is the number of surface groups per formula unit) exposed a large number of active sites with significant activation properties towards perovskite monosulfate (PMS)[23]. Based on MXene material, the composite catalysts are prepared by combining with transition metal oxides and monatomic transition metals. MXene based composites as catalysts for efficient decomposition of organic pollutants such as bisphenol A and salicylic acid in the presence of PMS[24]. These composites showed better activation performance under alkaline conditions, which may be related to the fact that alkaline conditions are favorable for accelerating the activation of PMS[25]. Although monatomic transition metals have higher activation effects, they are prone to deactivation by agglomeration[26]. Therefore, the anchoring of monatomic transition metals on the surface of MXene materials can enhance their stability[27]. Moreover, the incorporation of MXene simplified the coordination synthesis of monometallic atoms with the carrier and enhanced the removal performance of the catalysts for difficult organic

[1]College of Textile and Garments, Hebei University of Science and Technology, Shijiazhuang, Hebei 050018, China. [2]Hebei Jingze Textile Co., LTD, Handan, Hebei 050000, China. ✉e-mail: shudawu@126.com; fangfangan0312@163.com

pollutants[28]. Iron and its oxides are the most studied of the transition metal materials. Compared to other transition metals, they are environmentally friendly, relatively non-toxic and cost-effective. In addition, the special structure of MXene can confine the metal ions between its surface layers, effectively inhibiting the hydrolysis of Fe^{3+} and realizing the continuous activation of persulfate[29]. However, there are few reports on research related to MXene in reactive dyeing wastewater treatment.

C.I. Reactive Red 218 (RR218) was a monochlorotriazine reactive dye that was widely used in dyeing and inkjet printing of textiles. To investigate the role of MXene in the degradation of dyeing wastewater by Fe^{3+} activated sodium persulfate (SPS), the modeled dye solution of RR218 was used as the research object. The effects of SPS, Fe^{3+}, MXene concentration and pH value on the degradation of RR218 were investigated by testing the dye degradation rate. Additionally, the reduction performance of MXene towards Fe^{3+}, kinetics of RR218 degradation, dominant free radicals, and degradation mechanisms was thoroughly investigated. The potential for reuse of treated wastewater for dyeing was explored. This study provides a theoretical basis for the use of MXene in the degradation of dyeing wastewater.

Results

Morphology and elemental analysis of MXene

The morphologies of fresh and used MXene were observed using scanning electron microscopy (SEM) and are displayed in Fig.1a, b.

Figure 1a shows that the Ti_3AlC_2 MXene after 48 h etching treatment showed obvious layer structure. The surface and interlayers of the used MXene were filled with particles (Fig. 1b), which may be due to the deposition of substances or structural changes during the treatment of dyeing wastewater. The elemental composition of fresh and used MXene was investigated by EDS and the results are shown in Fig. 1c. Compared with the fresh MXene, the elemental of C and O increased by 24.33% and 1340.85%, respectively. The content of Ti decreased by 56.12% and 1.29% of Fe was introduced, which indicates that MXene was oxidized. A large number of Ti-O bonds were formed on the surface of the used MXene, and part of the Ti and Fe atoms were involved in the redox reaction. The surface of the used MXene becomes rough and the interlayers are filled with TiO_2 particles, which is consistent with the EDS results. This is due to the fact that MXene is oxidized by Fe^{3+} in the solution during operation, causing Ti_3C_2 to grow in situ to form TiO_2[30]. To compare the crystalline properties of MXene, the XRD data were given in Fig. 1d. The diffraction peaks at 8.8°, 18.0° and 60.1° of the fresh MXene coincide with the characteristic peaks of standard Ti_3C_2. Some of the diffraction peaks of used MXene were retained, while other diffraction peaks disappeared or decreased in intensity. This may be attributed to the particle structure attached to the surface of MXene, which decreased the crystallinity of the characteristic peaks by 1.13%. In addition, diffraction peaks appeared around 21.4°, 23.8°, and 26.6° for the used MXene, which contained characteristic peaks of Fe_2O_3 and TiO_2, as well as some pseudo-peaks due to the oxidation of Fe and Ti elements in MXene[31,32].

Degradation of RR218 in different conditions

To investigate the degradation properties of different reaction processes on RR218, the dye solution was treated at 25 °C for 0–30 min under the conditions of SPS of 3 g L^{-1}, Fe^{3+} of 3.35 mg L^{-1} and MXene concentration of 60 mg L^{-1}. The degradation rates of RR218 are shown in Fig. 2.

The maximum adsorption in 30 min was 2.1% when treating the dye solution with MXene only, which means that the adsorption of MXene can be ignored. The addition of Fe^{3+} to SPS increased the degradation rate of RR218 to 5.5%, which was attributed to the activation of SPS by Fe^{3+} (Eqs. (1) and (2)).

$$S_2O_8^{2-} + H_2O \rightarrow 2HSO_4^- + 2HSO_5^- \quad (1)$$

$$Fe^{3+} + HSO_5^- \rightarrow Fe^{2+} + SO_5^{\bullet -} + H^+ \quad (2)$$

For the system of SPS/MXene, the degradation of RR218 increased by 3 to 14% compared with its use alone, which may be attributed to the activation of SPS by MXene. Nevertheless, the degradation efficiency was still very low. When 3.35 mg L^{-1} Fe^{3+} was added into the SPS/MXene system, the degradation rate of RR218 reached 93.6% in 20 min, indicating that the Fe^{3+}/SPS/MXene process could effectively degrade RR218. The reason is that MXene promotes the conversion of Fe^{3+} to Fe^{2+}, thereby accelerating the activation of SPS. Besides, the MXene solution (after reaction) of filtration was clear and transparent, which was favorable for its reuse.

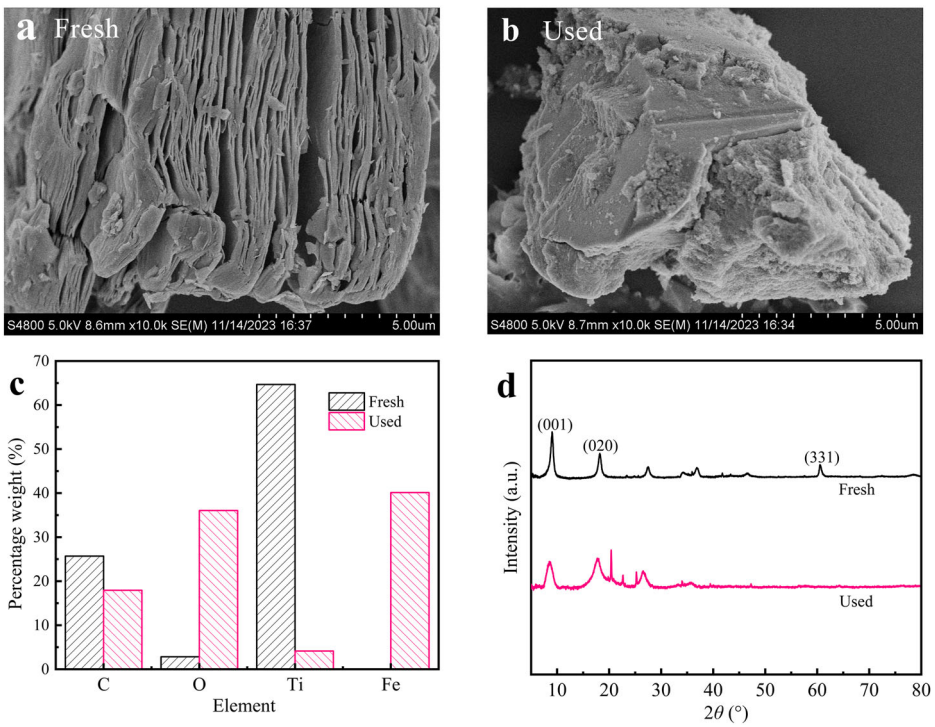

Fig. 1 | Characterization of MXene. SEM (**a**) and (**b**), EDS (**c**) and XRD (**d**) images of fresh and used MXene.

Factors affecting the degradation of RR218

To investigate the effect of SPS concentration on the degradation of RR218, 3.35 mg L^{-1} of Fe^{3+}, 60 mg L^{-1} of MXene and 1–4 g L^{-1} of SPS were added into the dye solution, then the mixed solution was treated at 25 °C for 0–30 min. The degradation rate curves of RR218 are shown in Fig. 3a.

RR218 untreated with SPS showed little degradation. The experimental data were fitted according to the quasi-primary kinetic model and the correlation coefficient $R^2 > 0.98$. This shows that the degradation curve of RR218 follows the quasi-primary reaction kinetics. When the concentration of SPS was increased from 1 g L^{-1} to 4 g L^{-1}, the degradation of RR218 increased with the higher concentration of SPS, and the degradation rate enhanced from 0.10 min^{-1} to 0.13 min^{-1}. At 30 min, the corresponding degradation of RR218 increased from 95.6% to 98.5%. The high concentration of SPS generates large amounts of $SO_4^{\bullet-}$ and ·OH, which leads to a higher degradation rate of RR218[33].

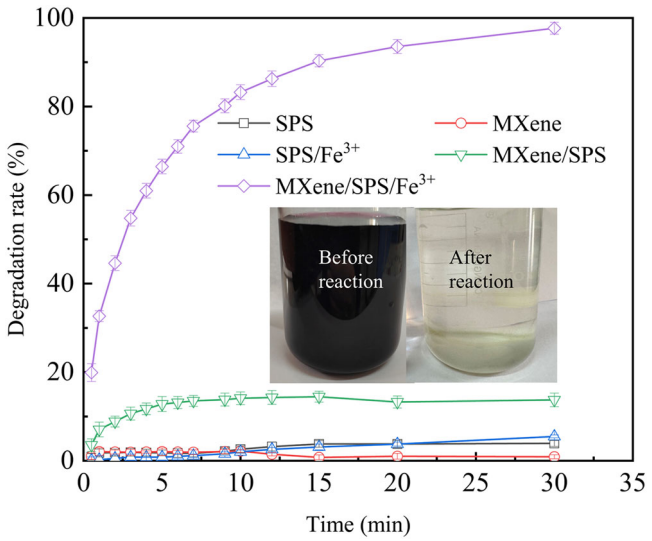

Fig. 2 | Role of different processes. Degradation rates of RR218 in different reaction processes.

The number of free radicals was closely related to the Fe^{3+} concentration at the constant SPS concentration. To reveal the relationship between Fe^{3+} concentration and the degradation rate of RR218, 1.67–16.75 mg L^{-1} of Fe^{3+} was added at the concentrations of 3 g L^{-1} and 60 mg L^{-1} of SPS and MXene, respectively. The sample was treated at 25 °C for 0–30 min. The degradation rate curves of RR218 are shown in Fig. 3b. In the Fe^{3+}/SPS/MXene medium, the degradation rate of RR218 showed a tendency to first increase and then decrease with the increase of Fe^{3+} concentration. When 3.35 mg L^{-1} of Fe^{3+} was added, the degradation rate of RR218 reached 97% at 30 min. The degradation rate of RR218 was increased from 0.12 min^{-1} to 0.20 min^{-1} by further increasing the Fe^{3+} concentration to 6.70 mg L^{-1}, which increased by about 66.67%. However, the degradation rate of RR218 showed a decreasing trend by continuing to enhance the Fe^{3+} concentration. This may be due to the high concentration of free radicals formed in the presence of excess catalyst, but the limited ability to react with the dye easily induces mutual quenching of the free radicals[34,35].

To elucidate the relationship between MXene concentration and the degradation efficiency of RR218, the dye solution was treated at 25 °C for 0–30 min under the conditions of 3 g L^{-1} of SPS, 3.35 mg L^{-1} of Fe^{3+} and 30–120 mg L^{-1} of MXene. The degradation rates are shown in Fig. 3c. Under the same treatment time, the higher the MXene concentration, the higher the degradation rate of RR218, which indicates that increasing the MXene concentration was favorable for the removal of dye in the wastewater. When the MXene concentration was increased from 30 mg L^{-1} to 120 mg L^{-1}, the degradation rate increased from 0.09 min^{-1} to 0.13 min^{-1}, which increased by 0.44 times. 98.9% degradation of RR218 could be achieved by stirring for 30 min when the concentration of MXene was 120 mg L^{-1}. The addition of MXene increased the degradation rate of RR218 by 60 times under the same condition of Fe^{3+}/SPS, which further confirmed that MXene played a significant role in the degradation of reactive dyes.

To reveal the effect of the initial pH on RR218 degradation, the pH of the dye solution was adjusted to 3, 5, 7, and 10, respectively, and all of them were added with 3 g L^{-1} of SPS, 3.35 mg L^{-1} of Fe^{3+} and 60 mg L^{-1} of MXene, and were treated at 25 °C for 0–30 min. The degradation rate of

Fig. 3 | Effects of different factors on degradation. Effect of SPS (**a**), Fe^{3+} (**b**), MXene (**c**) concentration and pH value (**d**) on RR218 degradation rate.

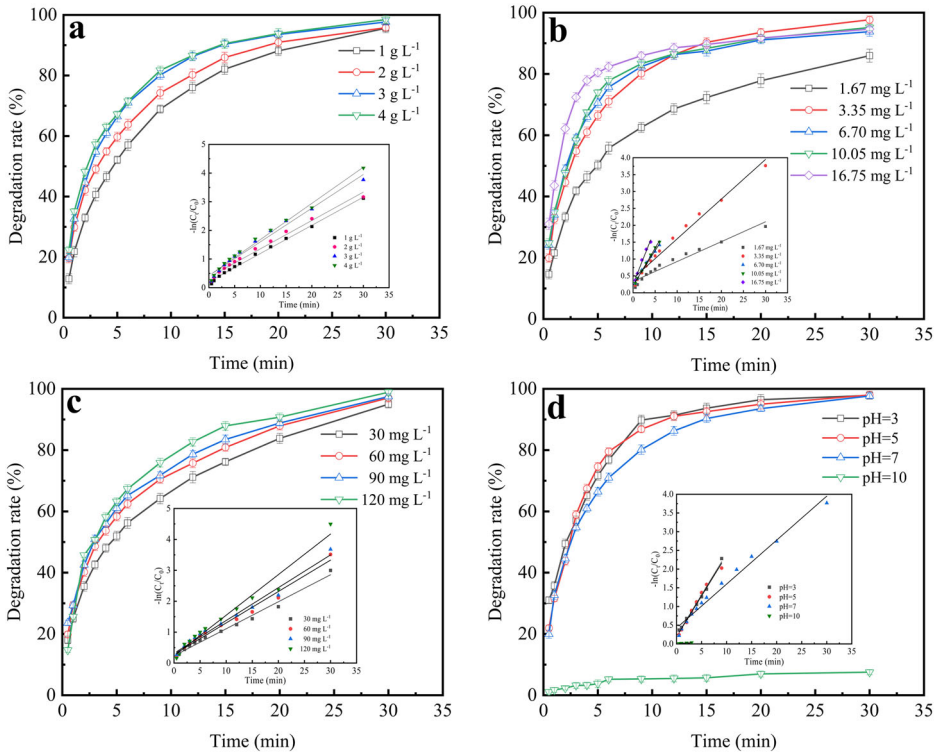

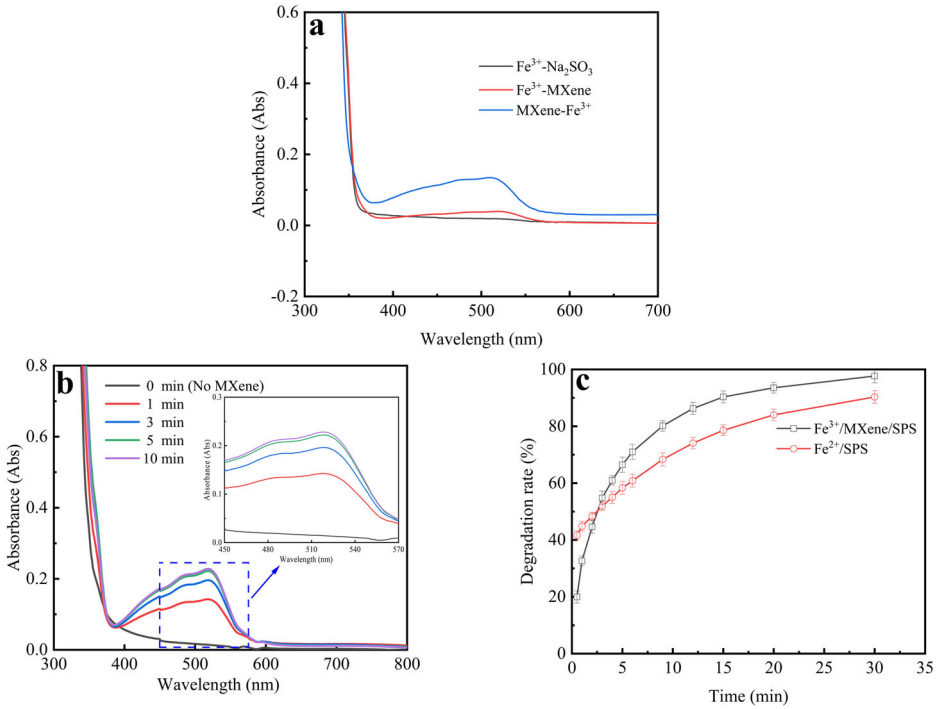

Fig. 4 | The role of MXene. UV-vis absorption spectra curves of Fe^{2+} in different processes (**a**), UV-vis spectra curves of Fe^{3+}/MXene at different times (**b**), degradation rates of RR218 in Fe^{2+}/SPS and Fe^{3+}/SPS/MXene system (**c**).

RR218 is shown in Fig. 3d. The degradation efficiency of RR218 decreased continuously when the solution pH increased from 3.0 to 10.0. Specifically, at pH = 3, the degradation rate of RR218 was 97.8% for 30 min of treatment, while at pH = 10, the degradation rate was only 7.5%. The degradation rate of RR218 showed a decreasing trend with the increase of pH. Under the alkaline condition, the iron ions were converted into precipitates and lost their catalytic ability to degrade the dye molecules effectively. The experimental data suggest that the pH should be adjusted to a neutral or acidic medium for the Fe^{3+}/SPS/MXene system.

Inhibition of Fe^{3+} hydrolysis

Fe^{3+} will be partially hydrolyzed to iron hydroxide under neutral conditions, and MXene can effectively prevent the hydrolysis of Fe^{3+} ions in water through its interlayer confinement effect. To investigate the inhibition effect of MXene on the hydrolysis of Fe^{3+}, experiments were carried out according to the experimental method (Fe^{3+} hydrolysis inhibition experiments).

As shown in Fig. 4a, the o-phenanthroline-Fe^{2+} complex in MXene-Fe^{3+} produced a significant absorption peak at 510 nm, while the Fe^{3+}-MXene absorption peak was weaker and no significant absorption peak was observed for Fe^{3+}-SPS. This phenomenon indicates that Fe^{2+} was produced in the MXene-Fe^{3+} process, and the other two groups of Fe^{3+} were due to the hydrolysis of the Fe^{3+} in neutral solution. The other two groups of Fe^{3+} were hydrolyzed in neutral solution and removed by filtration. The reason for this is that Fe^{3+} is easily hydrolyzed under neutral conditions, and most of the Fe^{3+} in the Fe^{3+}-SPS and Fe^{3+}-MXene processes were hydrolyzed to hydroxides, which were removed by membrane filtration. However, in the MXene-Fe^{3+} process, MXene can reduce Fe^{3+} to Fe^{2+}, and at the same time inhibit their hydrolysis by restricting both of them in its interlayer through the interlayer restriction domains[36]. The XRD plots of MXene before and after use (Fig. 1d) showed that the characteristic peaks before and after the reaction differed by 0.5. The decrease in the angle of the characteristic peaks also indicated the insertion of Fe^{3+} into the interlayer of MXene[29].

Reduction of Fe^{3+} to Fe^{2+}

To confirm that MXene can reduce Fe^{3+} to Fe^{2+}, it was trapped using o-phenanthroline, and the UV-Vis spectral curves presented in the Fe^{3+}/MXene mixture with time are shown in Fig. 4b. It can be seen that after the addition of MXene to $FeCl_3$ solution, the o-phenanthroline-Fe^{2+} complex produced an obvious absorption peak at 510 nm, confirming the reduction of Fe^{3+} to Fe^{2+} by MXene[37]. The degradation rates of RR218 in Fe^{2+}/SPS and Fe^{3+}/SPS/MXene in the presence of the same 3.35 mg L^{-1} of Fe^{3+} are given in Fig. 4c. In the Fe^{2+}/SPS process, RR218 was degraded rapidly in the first 30 s, and the degradation rate was as high as 53.90%, which was higher than that in the Fe^{3+}/SPS/MXene. However, the slow degradation of the dye after 30 s implies that in the first 30 s, part of the Fe^{2+} in the Fe^{2+}/SPS system was oxidized to Fe^{3+} by SPS and lost its catalytic ability. In contrast, in the Fe^{3+}/SPS/MXene system, the degradation rate of RR218 continued to increase with the treatment time, and the degradation rate at 30 min was 97.69%. The experimental results further confirmed that in the Fe^{3+}/SPS/MXene medium, MXene realized the Fe^{3+}/Fe^{2+} cycle, which was conducive to the activation of SPS and the degradation of RR218.

The elemental compositions of fresh and used Ti_3C_2 MXene are shown in Supplementary Table 1. Supplementary Table 1 illustrates that the elemental O content of Ti_3C_2 MXene increased from 22.37% to 49.71% after the use of Ti_3C_2 MXene, indicating that Ti_3C_2 MXene was oxidized. The XPS spectra of the used Ti_3C_2 MXene is shown in Fig. 5a, and the Fe 2p peak appeared at 710.6 eV. The Ti_3C_2 MXene Ti 2p XPS spectra before and after use are shown in Fig. 5b, c, where a large number of Ti-O bonds were generated after the reaction, resulting in the black MXene turning into a white precipitate (see Fig. 2). In addition, a small amount of Fe (3.50 at%) was observed in the XPS spectra, suggesting the existence of interfacial reaction between Fe^{3+} and MXene.

To further determine the evolution of Fe^{3+}, the high concentration of Fe^{3+} (6.70 mg L^{-1}) was analyzed by using XPS, and the results are shown in Fig. 5d. It can be seen that the obvious Fe $2p_{3/2}$ and Fe $2p_{1/2}$ peaks were observed at 710.2 eV and 723.8 eV after the use of MXene. Meanwhile, the Fe $2p_{3/2}$ peak of Fe^{2+} appeared at 710.0 eV, indicating that Fe^{3+} was reduced to Fe^{2+} by MXene[38]. The O 1 s XPS spectra of fresh and used MXene are shown in Fig. 5e, f. The three O 1 s peaks at 529.5 eV, 530.9 eV, and 532.1 eV correspond to Ti-O, C-Ti-O and Ti-OH bonds, respectively. In addition, a peak at 530.2 eV corresponding to the Fe-O bond appeared in the used MXene (Fig. 5f).

The reduction of Fe^{3+} by MXene was evaluated by o-phenanthroline spectrophotometry, and the results are shown in Fig. 6a.

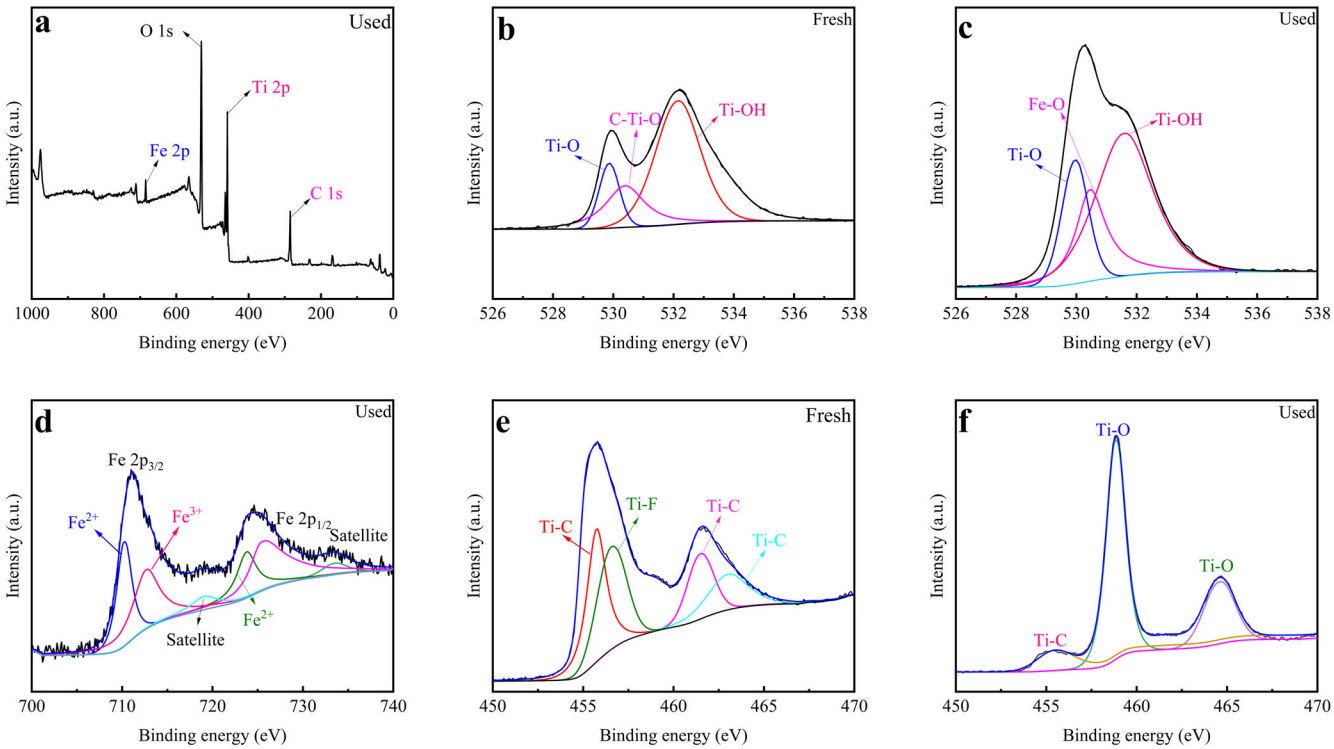

Fig. 5 | Element composition and variation on MXene. XPS spectra of used Ti_3C_2 MXene (**a**), fresh (**b**) and used (**c**) Ti_3C_2 MXene Ti 2p XPS spectra, Fe 2p (**d**) and O 1 s (**e**, **f**) XPS spectra.

Fig. 6 | Reduction capability of MXene. UV-Vis spectral curve of Fe^{3+} concentration and o-phenanthroline-Fe^{2+} complex (**a**), comparison of reduction performance of MXene and hydroxylamine (**b**).

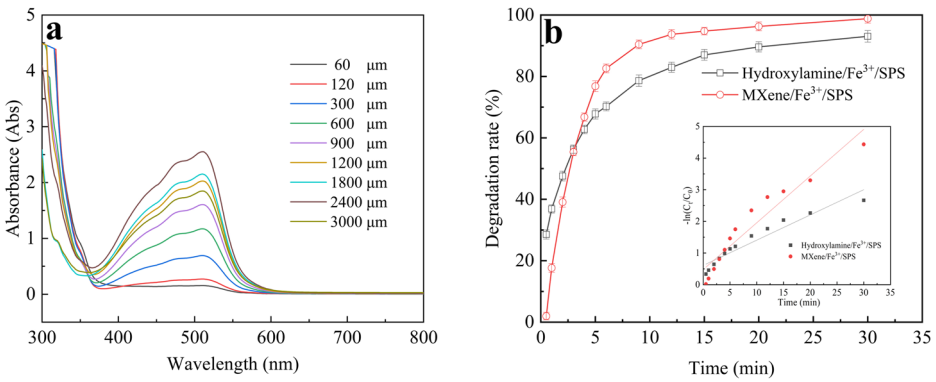

The addition of different concentrations of Fe^{3+} to the MXene process produced an absorption peak of o-phenanthroline-Fe^{2+} complex at around 510 nm, which confirmed the ability of MXene to reduce Fe^{3+}. When 2400 μM Fe^{3+} was added, the absorbance reached the maximum value, and the further increase of Fe^{3+} concentration did not increase the absorbance intensity, which indicated that the reducing ability of MXene in the process had been completely depleted at this time. The reducibility of Ti_3C_2 MXene originates from its exposed Ti atoms, and the complete oxidation of Ti atoms in Ti_3C_2 to TiO_2 will lose $4e^-$. Theoretically, 1 mol of Ti_3C_2 can reduce 4 mol of Fe^{3+} to Fe^{2+}, and 1 mol of hydroxylamine can only reduce 1 mol of Fe^{3+}[39,40]. To compare the reduction ability, the degradation rate curves of RR218 in Fe^{3+}/SPS process with the ratio of substance concentration of MXene and hydroxylamine of 1:4 are shown in Fig. 6b. The degradation rate of RR218 in Fe^{3+}/SPS/MXene process for 30 min was 6.19% higher than that in Fe^{3+}/SPS/hydroxylamine process. The degradation rate of the former was 0.15 min^{-1}, which is about 1.9 times that of the latter (0.08 min^{-1}), higher than the theoretical value of 1:1, further indicating that MXene possessed the ability to continuously reduce Fe^{3+}.

Degradation mechanism

The activation of SPS by Fe^{2+} tends to generate ·OH and $SO_4^{\bullet-}$, and their types and percentages directly affect the degradation of reactive dye. To investigate the roles of ·OH and $SO_4^{\bullet-}$ in the Fe^{3+}/SPS/MXene system, tert-butanol and methanol were used in excess as ·OH, $SO_4^{\bullet-}$ and ·OH quenchers, and the results were compared with those of the unspiked ones, which are shown in Fig. 7.

As shown in Fig. 7a, the degradation rate of RR218 was less than 7% when methanol was used as the quenching agent. In comparison, the degradation rate of the dye was increased to 8% when tert-butanol was used as the quenching agent, which was 93.51% and 91.83% lower than that of SPS, respectively. EPR experiments were conducted on reactive species in Fe^{3+}/SPS/MXene system using 5, 5-dimethyl-1-pyrroline N-oxide (DMPO) as the spin trap. As shown in Fig. 7b, the peak signals of DMPO-·OH and DMPO-$SO_4^{\bullet-}$ were detected simultaneously in the Fe^{3+}/SPS/MXene medium, confirming that the process did catalyze the activation of SPS to produce the above two radicals. The fitted pseudo-primary kinetic reaction rates are given in Supplementary Table 2. The percentage contributions of ·OH and $SO_4^{\bullet-}$ to the degradation of RR218 were 79.83% and 17.02%,

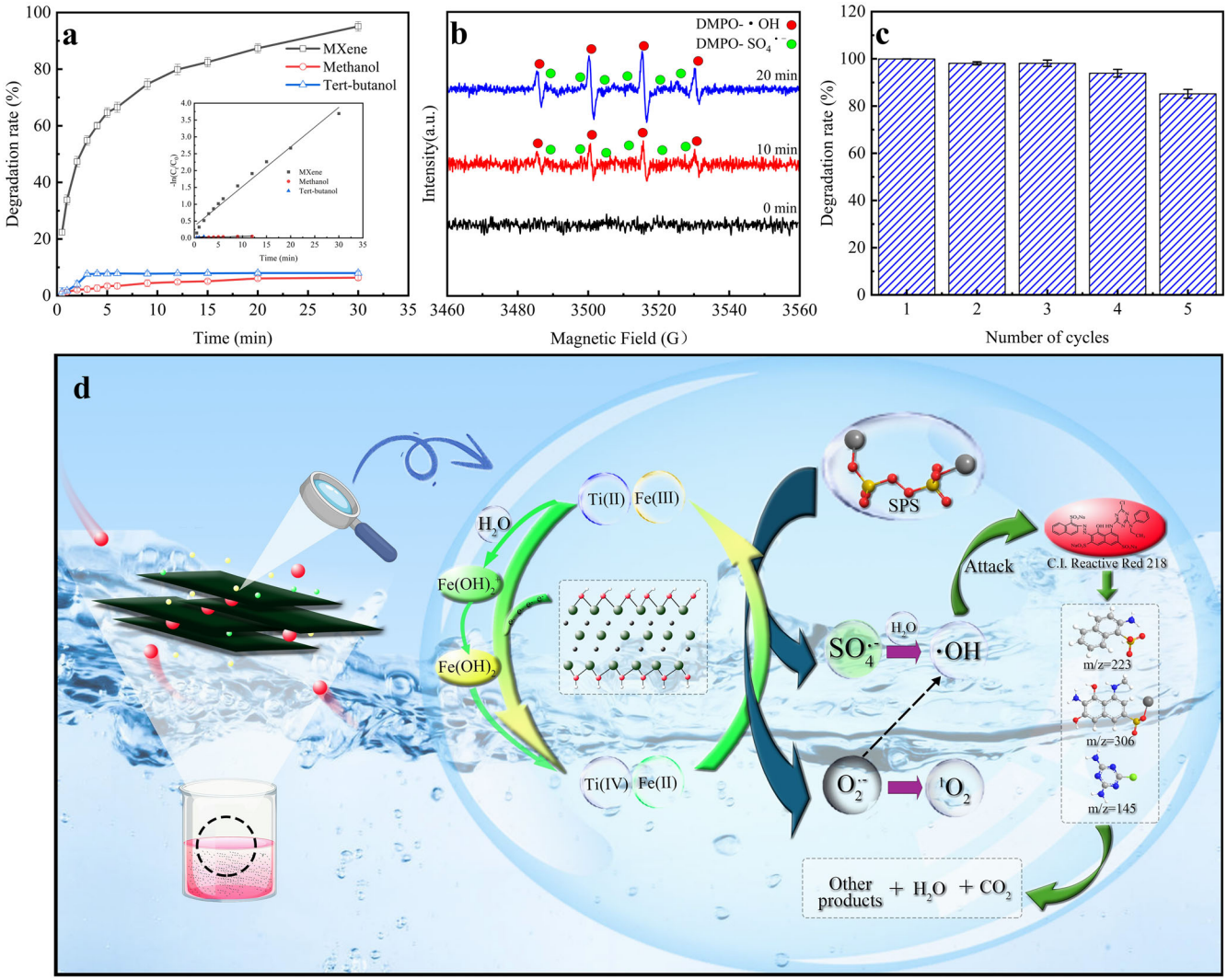

Fig. 7 | Reaction mechanism and material reuse performance. Relationship between free radical type and RR218 degradation rate (**a**), DMPO spin-trapping of Fe^{3+}/SPS/MXene process (**b**), the reusability of the material in the treatment of RR218 (**c**), schematic diagram of degradation mechanism (**d**).

respectively. The experiments showed that the degradation of RR218 in the Fe^{3+}/SPS/MXene process was a result of the synergistic action of ·OH and $SO_4^{\bullet-}$, but ·OH played a major role. To reveal the relationship between dye type and degradation rate, monochlorotriazine reactive dye (C.I. Reactive Red 24), monochlorotriazine-vinyl sulfone reactive dye (C.I. Reactive Red 195) and double vinyl sulfone reactive dye (C.I. Reactive Black 5) were selected for the experimental. The dye degradation rate curves are shown in Supplementary Fig. 1. At the same treatment conditions, the maximum degradation rate corresponding to C.I. Reactive Black 5 was 0.177 min^{-1}, the minimum for C.I. Reactive Red 195 was 0.135 min^{-1}, and the degradation rate for C.I. Reactive Red 24 was in between the previous two at 0.09 min^{-1}. When treated for 30 min, the degradation rates of these three dyes were all higher than 99%, indicating that the type of dye affects their degradation rate, but does not affect the final degradation. In terms of degradation rate, the fastest degradation was observed for the double vinyl sulfone structure, the slowest degradation was observed for the monochlorotriazine-vinyl sulfone mixed group, and the monochlorotriazine group was somewhere in between. As shown in Fig. 7c, the dye degradation rate showed a decreasing trend as the number of cycles increased. When the number of cycles was higher than 3, the dye degradation rate decreased more significantly, and the degradation rate of the 5th cycle was 85.17%, which was 14.77% lower than the 1st cycle.

In the Fe^{3+}/SPS/MXene system, the possible interactions are shown in Fig. 7d. Although MXene was a porous material with some adsorption properties, it only absorbed 2.1% RR218, which was negligible (Fig. 2). Ti_3C_2 loses $4e^-$ to form TiO_2, while Fe^{3+} will be converted to Fe^{2+} with the ability to activate SPS. In fact, there were also $Fe(OH)_2^+$ and $Fe(OH)_2$ substances formed in the solution as the pH increased (Fig. 7d)[41]. When the pH was higher than 7, $Fe(OH)_3$ precipitation was formed, the system Fe^{2+} concentration decreased, and the dye degradation rate was only 7.5% (shown in Fig. 3). After activation by Fe^{2+}, SPS formed ·OH as the main group, $SO_4^{\bullet-}$ as the auxiliary, and a small amount of $O_2^{\bullet-}$ and $^1O_2$ radicals. The free radicals act on the -N = N- and C-N bonds of reactive dyes to form intermediates containing naphthalene (m/z = 222.29 and m/z = 305.35), triazine (m/z = 144.11) structures (Supplementary Fig. 2), and ultimately formed small molecules such as CO_2 and H_2O[42,43].

Treatment and reuse of dyebath

In the preliminary studies, using SPS at concentrations of 3 g L^{-1}, Fe^{3+} at concentrations of 3.35 mg L^{-1}, MXene at concentrations of 60 mg L^{-1}, 25.0 °C, showed higher degradation efficiency. Cotton fabrics were dyed using the treated wastewater under this condition to explore the difference between the dyeing performance of treated wastewater and deionized water, and the dye uptake of RR218 was given in Fig. 8.

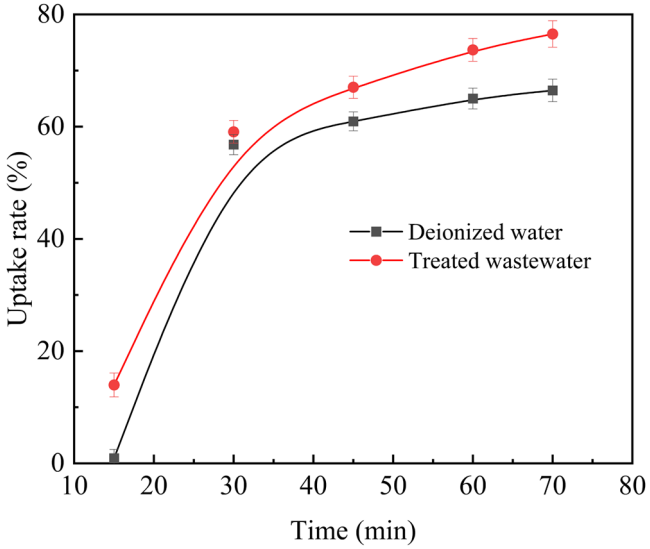

Fig. 8 | Reuse of dyebath. The uptake rate of RR218 in different dyeing media.

Table 1 | Color parameters of dyed fabrics and fixation of RR218

	*L**	*a**	*b**	*K/S*	*F%*
Conventional	61.11	40.92	−11.35	1.94	54.45
Reused	59.82	43.72	−10.96	2.42	62.67

Table 2 | Breaking strength and fastness properties of the dyed cotton fabrics[a] and COD of conventional dyeing and reused dyeing

Dyeing Process	Breaking stress (N)	Rubbing fastness		Washing fastness		COD (mg L^{-1})
		Dry	Wet	SC	SW	
Conventional	402.4	4–5	3	4–5	4–5	225.9
Reused	404.5	4–5	3	4–5	4–5	77.4

[a]Staining on cotton fabric (SC) and staining on wool fabric (SW).

The uptake of RR218 dyeing with treated wastewater can be divided into 2 stages: 0–30 min and 30–70 min. In the first stage, RR218 uptake increased rapidly to 59.1%. In the second stage, the dye uptake remained relatively stable with only a slow increase of 9.5%. The fabrics dyed with treated wastewater resulted in a higher dye uptake compared to that with deionized water. This is attributed to the fact that cations remain in the dye solution after filtration and act as dyeing promoters, weakening the electrostatic repulsion between dyes and fibers. To further compare the performance differences of the dyed fabrics, the fixation of RR218 as well as the color parameters of dyed fabrics are given in Table 1.

It can be seen that the fixation rate of RR218 dyed in recycled wastewater is 8.2% higher than that of conventional dyeing, indicating that recycled dyeing wastewater does not affect the utilization of dye. The small differences in the color parameters of the dyed fabrics further confirmed that the proposed recycled wastewater dyeing has good reproducibility and application prospects.

Table 2 shows the breaking stress, fastness properties, and COD of cotton fabrics dyed with conventional and reused dyeing processes. All dyed cotton fabrics exhibit excellent rubbing fastness and washing fastness. The breaking stress of fabrics dyed with the reused dyeing process was 2.1 N lower than that with conventional process. The COD of reused dyeing was reduced by about 65.7% compared to conventional dyeing.

Discussion

This study explored the rapid activation of sodium persulfate (SPS) for the degradation of C.I. Reactive Red 218 (RR218) using Ti_3C_2 MXene reduction of trace Fe^{3+} and investigated the wastewater reuse performance. The results showed that the suitable degradation conditions were 3 g L^{-1} of SPS, 3.35 mg L^{-1} of Fe^{3+} and 60 mg L^{-1} of MXene, and the degradation rate was as high as 97.7% when treated at 25 °C for 30 min. The strongly reducing MXene not only inhibits the hydrolysis of ferrous ions but also reduces Fe^{3+} to Fe^{2+} in a continuous cycle. When using the Fe^{3+}/SPS/MXene process for the degradation of RR218 wastewater, the percentage contributions of ·OH and $SO_4^{\bullet-}$ to the degradation of the dye were 78.71% and 17.97%, respectively. The dye degradation capacity of the Fe^{3+}/SPS/MXene process decreased after 5 cycles of recycling.

The treated bath was reused in dyeing process, observing good dyeing quality. This is attributed to the fact that the presence of cations weakens the electrostatic repulsion between the dyes and fibers, thus increasing the uptake rate. Ti_3C_2 MXene can be used to degrade reactive dyestuffs under neutral pH conditions by reducing Fe^{3+} activated sodium persulfate. The final precipitation of Ti_3C_2 MXene is non-toxic and can be removed by filtration, which will not cause secondary pollution. Overall, this study provides a method for the degradation and reuse of Ti_3C_2 MXene in dyeing wastewater.

Methods

Materials

The bleached cotton woven fabric (160 g m^{-2}) came from Hebei Ningfang Group Co., Ltd, China. Ti_3AlC_2 powder (400 mesh) was purchased from Shanghai Macklin Biochemical Technology Co., Ltd. Iron trichloride ($FeCl_3$), ferrous sulfate ($FeSO_4{\cdot}7H_2O$), sulfuric acid (H_2SO_4) and sodium hydroxide (NaOH), Methanol (MeOH, CH_3OH), tert-Butyl alcohol (TBA, $C_4H_{10}O$), sodium thiosulfate (ST, $Na_2S_2O_3$) and sodium persulfate (SPS, $Na_2S_2O_8$) were purchased from Tianjin Oubokai Chemical Co., Ltd. Hydroxylamine hydrochloride ($NH_2OH{\cdot}HCl$), ammonium acetate (CH_3COONH_4), and phenanthroline ($C_{12}H_8N_2$) were purchased from Shanghai Aladdin Biochemical Technology Co., Ltd. The chemicals were analytical grade without further purification. C.I. Reactive Red 218 (RR218), C.I. Reactive Red 24 (RR24), C.I. Reactive Red 195 (RR195) and C.I. Reactive Black 5 (RB5) for salt-free inkjet were purchased from Jiangsu Shenxin Dyestuff Chemical Co., Ltd. The structural formula of reactive dyes is shown in Supplementary Fig. 3.

Preparation of Ti_3C_2 MXene

Ti_3C_2 MXene was prepared according to the reported HCl/LiF method[44]. 2 g of Ti_3AlC_2 ceramic powder was slowly added to 40 mL of a mixed solution of HCl (9 mol L^{-1}) and LiF, and the reaction was carried out in a water bath at 40 °C for 48 h. Excess LiF was removed by washing with dilute hydrochloric acid (1 mol L^{-1}), and then the mixture was washed with ultrapure water and centrifuged at 3500 rpm for 5 min. The reaction was repeated several times until the pH of the supernatant was greater than 6. The precipitate was collected and dried under a vacuum at 60 °C for 48 h.

Wastewater treatment

All discoloration tests were performed in triplicate, using a digital display constant temperature water bath pot (HH-S4, Changzhou Guoyu Instrument Manufacturing Co., Ltd). In the experiment, 100 mL of dyeing wastewater (0.05 g L^{-1}) was added to sodium persulfate solutions and in concentrations of 1–4 g L^{-1}, followed by 30–120 mg L^{-1} MXene and 1.67–16.75 mg L^{-1} Fe^{3+}, and the degradation experiments were carried out at 25 °C. The solution pH was adjusted by H_2SO_4 (0.01 mol L^{-1}) and NaOH (0.01 mol L^{-1}). Degradation rates were analyzed by UV-Vis spectrophotometry on UV-3200 equipment (Shanghai Mapada Instrument Co. LTD), based on absorbance values recorded at 547 nm.

At the end of the wastewater treatment experiment, the MXene material was filtered using a 0.22 μm membrane. The pollutants on the surface of the material were removed by repeated rinsing with ethanol and

deionized water. Subsequently, the material was placed in a vacuum oven at 60 °C for 48 h. After the drying process was completed, the material was subjected to reusability experiments.

Fe^{3+} hydrolysis inhibition experiments

Different reductants MXene and Na_2SO_3 were selected and divided into three groups according to the order of addition. 3.35 mg L^{-1} Fe^{3+} was added to the first and second groups respectively. Na_2SO_3 and MXene were added after 10 min of reaction, while equal amounts of MXene and Fe^{3+} were added to the third group successively. After 10 min of reaction, 4 mL of the solution was taken from each group and filtered through a 0.22 μm membrane. The UV-Vis absorption spectra were recorded after 15 min with the addition of o-phenanthroline and ammonium acetate to the three filtrates.

Reuse of dyeing solution

The dyeing process was designed in Supplementary Fig. 4. Dyeing was performed on an HT-B-24 dyeing machine (Guangdong Heshan Hongfa Dyeing and Finishing Machinery Manufacturing Co., Ltd) with a capacity of 150 mL. Initially, 2.0 g of 100% bleached cotton was immersed in the dyeing bath containing 60 mL of treated dyeing solution or deionized water (bath ratio of 30:1), 0.5%(o.w.f) of RR218. Then, the bath temperature was increased to 40.0 °C and maintained for 15 min. After 15 min, 60 g L^{-1} of NaCl was added to the bath, remaining at 40.0 °C for another 15 min. Then, the dyeing temperature was raised to 60 °C, and 20 g L^{-1} of Na_2CO_3 was added to the dyeing solution, remaining at 60.0 °C for 40 min. After dyeing, the dyed fabric sample was washed and then dried.

Analytical techniques

SEM (Hitachi S4800, Japan) and energy spectrum analyzer (EDS) were used to test the surface micromorphology and elemental content of the samples. The physical composition of the materials was characterized by X-ray diffraction (XRD, Rigaku Miniflex600, Japan). The active radicals (hydroxyl and sulfate radicals) were detected by spin trapping with DMPO (4.00 mmol L^{-1}) in an EPR spectrometer (Bruker EMX PLUS, Germany). Elemental composition and valence information were determined by X-ray photoelectron spectroscopy (XPS, Thermo Fisher Scientific, USA). Dye degradation products were analyzed using an Ultra-high performance liquid chromatography (HPLC-MS) (LC, Shimadzu LC-30A, Japan; MS, AB SCIEX Triple TOFTM 5600+four stage time-of-flight mass spectrometer). Chemical oxygen demand (COD) was measured by using a COD rapid analyzer (LY-C3, Qingdao Lvyu Environmental Protection Technology Co., Ltd., China).

Kinetic analysis of degradation reaction

Degradation of the dyeing solution was calculated according to Eq. (3). Take the reaction time as the horizontal coordinate and $\ln(C_t/C_0)$ as the vertical coordinate to obtain the linear equation of the reaction rate. The slope of this equation represents the kinetic reaction rate constant.

$$\text{Degradation}(\%) = \left(1 - \frac{C_t}{C_0}\right) \times 100\% \quad (3)$$

Where C_t represents the absorbance during soaping at a specified time and C_0 is the initial absorbance.

Dyeing properties

The exhaustion (E) and fixation rate (F) of RR195 were calculated using Eq. (4) and Eq. (5), respectively.

$$E(\%) = \left(1 - \frac{b \times A_t}{a \times A_0}\right) \times 100\% \quad (4)$$

$$F(\%) = \left(\frac{a \times A_0 - c \times A_1 - d \times A_2}{a \times A_0}\right) \times 100\% \quad (5)$$

Where, A_0 and A_t are the absorbance of dye solution at 0 and t min of dyeing. a and b are the dilution ratios of the dye solution. A_1 and A_2 are the absorbance of solutions at the end of the dyeing and soaping process. c and d are the dilution ratios corresponding to the end of dyeing and the soaping.

The color parameters were tested according to the published literature[45].

The rubbing and washing fastness of dyed fabrics were measured according to ISO 105-X12: 2016 and ISO 105-C10: 2007, respectively.

Data availability

The authors confirm the data supporting the findings of the study are found within the main article and the Supporting Information. Additional data pertaining to the study may be requested from the authors.

Received: 7 January 2024; Accepted: 17 April 2024;
Published online: 26 April 2024

References

1. Song, Y. et al. An overview of biological mechanisms and strategies for treating wastewater from printing and dyeing processes. *J. Water Process. Eng.* **55**, 104242 (2023).
2. Gu, P. et al. Recent strategies, progress, and prospects of two-dimensional metal carbides (MXenes) materials in wastewater purification: a review. *Sci. Total. Environ.* **912**, 169533 (2024).
3. Zhao, Y. et al. COF-based membranes for liquid phase separation: Preparation, mechanism, and perspective. *J. Environ. Sci.* **141**, 63–89 (2024).
4. Ghaffar, A. et al. Electrospun silk nanofibers for numerous adsorption-desorption cycles on Reactive Black 5 and reuse dye for textile coloration. *J. Environ. Chem. Eng.* **11**, 111188 (2023).
5. Khattab, T. A., Abdelrahman, M. S. & Rehan, M. Textile dyeing industry: environmental impacts and remediation. *Environ. Sci. Pollut. R.* **27**, 3803–3818 (2020).
6. Parvin, F., Islam, S., Urmy, Z., Ahmed, S. & Islam, A. S. A study on the solutions of environment pollutions and worker's health problems caused by textile manufacturing operations. *Biomed. J. Sci. Tech. Res.* **28**, 21831–21844 (2020).
7. Jiang, Z. et al. Recent advances and perspectives of emerging two-dimensional transition metal carbide/nitride-based materials for organic pollutant photocatalysis. *Mater. Chem. Front.* **7**, 4658–4682 (2023).
8. Chen, P. et al. Efficient degradation of dye wastewater by catalytic ozonation reactive ceramic membrane with facile spraying of nano TiMn oxides: a pilot scale attempt. *J. Water Process. Eng.* **55**, 104143 (2023).
9. Chen, Q., Yao, Y., Zhao, Z., Zhou, J. & Chen, Z. Long term catalytic activity of pyrite in Heterogeneous Fenton-like oxidation for the tertiary treatment of dyeing wastewater. *J. Environ. Chem. Eng.* **9**, 105730 (2021).
10. Wang, Y. et al. Potassium permanganate-based advanced oxidation processes for wastewater decontamination and sludge treatment: a review. *Chem. Eng. J.* **452**, 139529 (2023).
11. Yang, Y. et al. Insight into the application of micro-nano bubbles combined with heat-activated persulfate oxidation for removing dissolved organic matter from printing and dying wastewater. *J. Water Process. Eng.* **56**, 104463 (2023).
12. Nidheesh, P. V., Divyapriya, G., Ezzahra Titchou, F. & Hamdani, M. Treatment of textile wastewater by sulfate radical based advanced oxidation processes. *Sep. Purif. Technol.* **293**, 121115 (2022).
13. Arvaniti, O. S., Ioannidi, A. A., Mantzavinos, D. & Frontistis, Z. Heat-activated persulfate for the degradation of micropollutants in water: a comprehensive review and future perspectives. *J. Environ. Manag.* **318**, 115568 (2022).
14. Van Tri, D., Barcelo, D. & Le Luu, T. The performances of persulfate activators to degrade the persistent organic pollutants in industrial wastewater. *Case. Stud. Chem. Environ. Eng.* **8**, 100539 (2023).

15. Wang, B. & Wang, Y. A comprehensive review on persulfate activation treatment of wastewater. *Sci. Total. Environ.* **831**, 154906 (2022).
16. Sonawane, S., Rayaroth, M. P., Landge, V. K., Fedorov, K. & Boczkaj, G. Thermally activated persulfate-based advanced Oxidation Processes — recent progress and challenges in mineralization of persistent organic chemicals: a review. *Curr. Opin. Chem. Eng.* **37**, 100839 (2022).
17. Kodavatiganti, S., Bhat, A. P. & Gogate, P. R. Intensified degradation of Acid Violet 7 dye using ultrasound combined with hydrogen peroxide, Fenton, and persulfate. *Sep. Purif. Technol.* **279**, 119673 (2021).
18. Xiao, S. et al. Iron-mediated activation of persulfate and peroxymonosulfate in both homogeneous and heterogeneous ways: a review. *Chem. Eng. J.* **384**, 123265 (2020).
19. Tang, Y., Dou, J., Lu, Z., Xu, J. & He, Y. Accelerating Fe^{2+}/Fe^{3+} cycle via biochar to improve catalytic degradation efficiency of the Fe^{3+}/persulfate oxidation. *Environ. Pollut.* **316**, 120669 (2023).
20. Miao, F. et al. Electro-enhanced heterogeneous activation of peroxymonosulfate via acceleration of Fe(III)/Fe(II) redox cycle on Fe-B catalyst. *Electrochim. Acta* **377**, 138073 (2021).
21. Karthikeyan, P. et al. Effective removal of Cr(VI) and methyl orange from the aqueous environment using two-dimensional (2D) $Ti_3C_2T_x$ MXene nanosheets. *Ceram. Int.* **47**, 3692–3698 (2021).
22. Zhang, Z., Xu, J. & Yang, X. MXene/sodium alginate gel beads for adsorption of methylene blue. *Mater. Chem. Phys.* **260**, 124123 (2021).
23. Guo, X. et al. Derivatives of two-dimensional MXene-MOFs heterostructure for boosting peroxymonosulfate activation: enhanced performance and synergistic mechanism. *Appl. Catal. B-Environ.* **323**, 122136 (2023).
24. Ding, M. et al. Novel α-Fe_2O_3/MXene nanocomposite as heterogeneous activator of peroxymonosulfate for the degradation of salicylic acid. *J. Hazard. Mater.* **382**, 121064 (2020).
25. Song, H. et al. Anchoring single atom cobalt on two-dimensional MXene for activation of peroxymonosulfate. *Appl. Catal. B-Environ.* **286**, 119898 (2021).
26. Crabtree, R. H. Deactivation in homogeneous transition metal catalysis: causes, avoidance, and cure. *Chem. Rev.* **115**, 127–150 (2015).
27. Liu, X., Li, C., Xu, F., Fan, G. & Xu, H. Density functional theory study of nitrogen-doped black phosphorene doped with monatomic transition metals as high performance electrocatalysts for N_2 reduction reaction. *Nanotechnology* **33**, 245401 (2022).
28. Li, W. et al. Peroxymonosulfate activation by oxygen vacancies-enriched MXene nano-Co_3O_4 co-catalyst for efficient degradation of refractory organic matter: Efficiency, mechanism, and stability. *J. Hazard. Mater.* **432**, 128719 (2022).
29. Song, H. et al. Enhanced photocatalytic degradation of perfluorooctanoic acid by Ti_3C_2 MXene-derived heterojunction photocatalyst: Application of intercalation strategy in DESs. *Sci. Total. Environ.* **746**, 141009 (2020).
30. Low, J., Zhang, L., Tong, T., Shen, B. & Yu, J. TiO_2/MXene Ti_3C_2 composite with excellent photocatalytic CO_2 reduction activity. *J. Catal.* **361**, 255–266 (2018).
31. Zhao, N. et al. Fe^{3+}-stabilized $Ti_3C_2T_x$ MXene enables ultrastable Li-ion storage at low temperature. *J. Mater. Sci. Technol.* **67**, 156–164 (2021).
32. Tan, Q. et al. Photo-Fenton properties of MIL-88A(Fe) / Ti_3C_2 MXene with tunable active crystal facets: Universal for degradation of common pollutants in wastewater. *Process. Saf. Environ.* **179**, 405–420 (2023).
33. Kermani, M. et al. Degradation of furfural in aqueous solution using activated persulfate and peroxymonosulfate by ultrasound irradiation. *J. Environ. Manag.* **266**, 110616 (2020).
34. Dong, Z., Zhang, Q., Chen, B. & Hong, J. Oxidation of bisphenol A by persulfate via Fe_3O_4-α-MnO_2 nanoflower-like catalyst: mechanism and efficiency. *Chem. Eng. J.* **357**, 337–347 (2019).
35. Ouyang, D. et al. Degradation of 1,4-dioxane by biochar supported nano magnetite particles activating persulfate. *Chemosphere* **184**, 609–617 (2017).
36. Han, W. et al. Activating an MXene as a host for $EMIm^+$ by electrochemistry-driven Fe-ion pre-intercalation. *J. Mater. Chem.* **8**, 16265–16270 (2020).
37. Yang, Z., Yan, Y., Yu, A., Pan, B. & Pignatello, J. J. Revisiting the phenanthroline and ferrozine colorimetric methods for quantification of Fe(II) in Fenton reactions. *Chem. Eng. J.* **391**, 123592 (2020).
38. Ma, Y., Lv, X., Xiong, D., Zhao, X. & Zhang, Z. Catalytic degradation of ranitidine using novel magnetic Ti_3C_2-based MXene nanosheets modified with nanoscale zero-valent iron particles. *Appl. Catal. B-Environ.* **284**, 119720 (2021).
39. Li, Z. et al. Further understanding the role of hydroxylamine in transformation of reactive species in Fe(II)/peroxydisulfate system. *Chem. Eng. J.* **418**, 129464 (2021).
40. Wang, L. et al. Effective removal of anionic Re(VII) by surface-modified Ti_2CT_x MXene nanocomposites: Implications for Tc(VII) sequestration. *Environ. Sci. Technol.* **53**, 3739–3747 (2019).
41. Song, H. et al. Ultrafast activation of peroxymonosulfate by reduction of trace Fe^{3+} with Ti_3C_2 MXene under neutral and alkaline conditions: reducibility and confinement effect. *Chem. Eng. J.* **423**, 130012 (2021).
42. Qiu, Y. et al. Degradation of anthraquinone dye reactive blue 19 using persulfate activated with Fe/Mn modified biochar: radical/non-radical mechanisms and fixed-bed reactor study. *Sci. Total. Environ.* **758**, 143584 (2021).
43. Basilio, A. O. et al. Degradation of reactive dyes by thermally activated persulfate and reuse of treated textile dye-bath. *J. Braz. Chem. Soc.* **32**, 1865–1873 (2021).
44. Alhabeb, M. et al. Guidelines for synthesis and processing of two-dimensional titanium carbide ($Ti_3C_2T_x$ MXene). *Chem. Mater.* **29**, 7633–7644 (2017).
45. Shu, D. et al. Cleaner pad-steam dyeing technology for cotton fabrics with excellent utilization of reactive dye. *J. Clean. Prod.* **241**, 118370 (2019).

Acknowledgements

This work was supported by Youth Foundation of Hebei Province Department of Education Fund (QN2023090) and Hebei Natural Science Foundation (B2020208061).

Author contributions

D.S. put forward the experimental idea; W.L. designed and performed the experiments, and drafted the manuscript; F.A. and R.L. performed the characterization; J.S., B.H., and S.C. supervised the data analysis.

Competing interests

The authors declare no competing interests.

Additional information

Supplementary information The online version contains supplementary material available at https://doi.org/10.1038/s41545-024-00330-9.

Correspondence and requests for materials should be addressed to Dawu Shu or Fangfang An.